Development of Unmanned Airboat for Water-Quality Mapping

Yutaka Kaizu[a,*], Munetaka Iio[b], Hiroyuki Yamada[a], Noboru Noguchi[a]

[a]*Research Faculty of Agriculture, Hokkaido University, Kita-9, Nishi-9, Kita-ku, Sapporo, Hokkaido, Japan*

[b]*Graduate School of Agriculture, Hokkaido University, Kita-9, Nishi-9, Kita-ku, Sapporo, Hokkaido, Japan*

[*] *Corresponding author. Tel.: +81 11 706 2568; fax: +81 11 706 2568.*

E-mail address: yuta_kaizu@yahoo.co.jp (Yutaka Kaizu)

Kita-9, Nishi-9, Kita-ku, Sapporo, Hokkaido, Japan 060-8589

Abstract: We have developed an unmanned airboat for mapping the water quality of shallow (<1 m) mire pools where aquatic weeds flourish. A differential global positioning system receiver and a global positioning system compass were used as navigation sensors. The airboat was designed for automatic operation. Using the boat, we measured parameters such as temperature, pH, dissolved oxygen, electrical conductivity, turbidity and chlorophyll-a of the water in a 26-ha mire pool in Hokkaido, Japan. To determine the appropriate sampling-grid size, the water was sampled along lines spaced 10 m apart, and the spatial variability of the mire pool characteristics was determined using a semivariogram. Results from the spherical model fit to the empirical semivariogram revealed spatial fluctuations in the water-quality parameters on the scale of 100 to 140 m. Because the size of the grid must be smaller than this scale, a second survey of water samples in the pool was carried out using a grid size of 40 m × 40 m. At each target point, a water-quality sensor unit was lowered from the boat. The survey of the entire grid area took approximately 231 min, during which time 130 points were sampled. The precision of the sampling points was within 2.6 m. The maximum speed and yaw rate of the airboat were 1.2 m s^{-1} and 48 deg s^{-1}, respectively. The resulting maps showed the fine-scale distribution of water quality.

Keywords: *Water quality, Grid sampling, Unmanned surface vessel, Navigation, Yaw rate, Semivariogram*

Nomenclature

D	distance between boat and target point, m
h	distance between two sampling points in semivariogram, m
K_d	derivative gain, dimensionless
K_p	proportional gain, dimensionless
r_1	radial distance at which the fans are stopped, m
r_2	radial distance at which the maximum rotational speed is controlled, m
R_d	relative rotational speed of two fans, rpm
R_l	rotational speed of left fan, rpm
$R_{\max}$	maximum rotational speed of either of the two (left or right) fans, rpm
R_r	rotational speed of right fan, rpm
V	speed of the boat, m s^{-1}
X	axis parallel to the Easting line of the UTM coordinate system
Y	axis parallel to the Northing line of the UTM coordinate system
β	drift angle, degrees
ψ	heading of the boat, degrees
ψ_b	bearing of the target points from the boat, degrees
ψ_r	relative bearing, degrees
$\dot{\psi}_r$	first derivative of relative bearing, degrees s^{-1}

1. INTRODUCTION

1.1 Background

Inland water bodies such as lakes, mire pools, rivers and ponds are useful in flood control, fisheries, recreation and as fresh water sources. Environmental protection of such water bodies has been given increasing importance recently, especially because such areas provide habitats for many wild animals and plants. However, the conservation and sustainable management of inland water bodies pose significant challenges because lakes or swamps located at the end of catchment basins form semi-closed water bodies, leading to the rapid accumulation of sludge. Therefore, many small lakes in Japan do not meet water-quality standards. It has been reported that lakes surrounded by farming areas, in particular, are polluted (T. Kizuka, Yamada, Yazawa, & Chung, 2008).

Water quality of a lake can be modelled by measuring the inflow and outflow quantities and also by taking water samples. To obtain a precise model, the sampling-time interval should be as short as possible. When spatial variations in water quality are expected, sampling should be performed at many points across the entire lake. In practice, however, constraints involving time, cost and human labour limit the sampling interval and spatial resolution that can be attained. To obtain a high-resolution water-quality measurement of a lake, a mobile, low-cost and unmanned measurement platform is desirable.

1.2 Existing water-sampling methods

At present, the assessment of water quality of lakes is generally performed using a manned boat. For cases where the lake bed is deeper than the depth of a propeller and when there are no aquatic weeds near the water surface, a conventional propeller is the best propulsion method. On the other hand, shallow lakes such as mire pools having aquatic weeds require a row boat. However, when there are winds, it is difficult to row a boat to various target points on the lake. From our experience, when the wind speed is as low as 5 m s^{-1}, it is extremely difficult to row an inflatable rubber boat in the windward direction. The sampled water is bottled and subsequently analysed either in a laboratory or is measured onsite by using a water-quality sensor unit. For both methods, the sampling positions are recorded using a global positioning system (GPS) so that the maps showing variations in the water-quality parameters with position may be constructed afterwards.

Until now, various unmanned surface vessels (USVs) have been developed for military purposes, geographical surveillance of the sea floor or water assessment. Li and Weeks (2009) utilised a USV to measure water currents and to analyze an eddy. David et al. (2007) used a commercial USV to create a three-dimensional map of an oyster habitat in Apalachicola Bay, Florida; this GPS-navigated USV proved very useful for mapping the shallow coast. Singh et al. (2008) developed a remote-controlled airboat that measures the depth of a sludge layer in a lagoon. This airboat was equipped with differential GPS (DGPS) and side-scan sonar for mapping the bottom of the lagoon. However, this boat was not fully automated. In another study, Singh et al. (2007) developed a small robotic airboat to investigate the water quality of a small lake. This boat was navigated automatically via GPS and a compass. It differs from the boat presented in our study in that it was operated using an electric motor and was smaller.

An airboat is a vessel that is propelled by onboard fans. It has a flat bottom, allowing it to cruise in shallow waters. The propulsion force of an airboat is smaller and the cruising speed is slower as compared to a propeller-driven boat with a similar-sized engine. However, an airboat has the critical advantage of not requiring underwater propellers, which may get entangled in aquatic weeds. Another advantage of an airboat is that there is less disturbance from the mud at the bottom of the lake and at the water surface. Therefore, an airboat is a good option for obtaining measurements in shallow waters.

1.3 Objectives

The objectives of this study are as follows:

- Develop an unmanned airboat that has optimal dynamic control, automatically navigates to predefined sampling points and measures specific water-quality indices such as pH, dissolved oxygen (DO), electrical conductivity (EC), turbidity, temperature, depth of the sensor unit, water depth, concentration of chlorophyll-a and NO_3 ions.
- Prepare high-resolution maps that display spatial variations in water-quality indices for the mire pool.

2. MATERIALS AND METHODS

2.1 Unmanned Airboat

An unmanned boat platform (Fig. 1) was developed to sample the water in a mire pool over a grid pattern. The main body of the platform was a float boat (Car Mate Mfg. Co., Ltd., model Z1). This fishing boat had two floats on each side, and the payload was 150 kg. The boat was equipped with two four-cycle gasoline engines (Makita Numazu Company, model EH035). The maximum power output of each engine was 1.2 kW and the maximum rotational speed of the output shaft was 7000 rpm. The driving force was generated by two 35-cm-diameter fans. To control the rotational speed of the engines, the throttles were connected to radio-controlled (RC) servo motors. The rotational speed of each engine was measured using proximity sensors attached to the fan axles. The capacity of the gasoline tank was 5 l, enabling the boat to be operated for 6 h at maximum engine output. However, since the engines had no reverse gear, the boat was carefully navigated in order to prevent it from running aground.

The boat was navigated using a Hemisphere V100 GPS compass, which included two DGPS receivers, so that it could measure the heading angle. The precision of the horizontal position and the heading angle were 0.6 m and 0.3°, respectively. The data-transmission frequency was 20 Hz. A water-quality sensor unit (DKK-TOA Corporation, model WQC-24) was attached to the bow of the airboat to measure the water surface before it was disturbed by the body of the boat. This multi-sensor unit measured pH, DO, EC, turbidity, temperature, depth of the sensor unit, concentration of chlorophyll-a and NO_3 ions. A 12-V winch that was controlled by a single-board computer (Atmel Corporation, Model ATmega168) (Banzi, 2009) was responsible for raising and lowering the sensor unit. The sensor was raised when the boat was cruising, so that its motion was unhindered, and was lowered when the boat reached the targeted sampling spot. An internet-protocol camera was used to observe the surroundings of the boat. To allow the boat's status to be observed from the shore, a non-directional 2.4-GHz wireless local area network (WLAN) antenna (Buffalo, Inc., model WLE-HG-NDC) was attached to the boat.

A similar type of WLAN antenna was also used at the surveillance base in order to enable communication with the boat up to the range of 500 m from the base. A sonar transducer was positioned at the stern of the boat to record the depth of the lake; however, we do not discuss those sonar results because the bottom of the lake was covered with plants, making accurate readings difficult.

(Fig. 1. Unmanned boat platform.)

Figure 2 shows a schematic diagram of the system. The rotational speed of the engines was controlled using feedback. Every second, a laptop computer on the boat sent rotation messages to the ECU in order to control the RC servo motors. The rotary encoder counted the number of rotations made by the winch while lowering the sensor to the designated depth. The depth of the sensor unit and its submersion time were configurable. The program used to record the data and navigate the boat was developed using National Instruments LabVIEW 2009, and was continuously running on the laptop that was placed in the boat. The boat's laptop was remotely controlled by another laptop at the surveillance base by using Microsoft Remote desktop connection. Software provided by the sensor manufacturer, DKK-TOA Corporation, was used to record the data obtained from the water-quality sensor.

(Fig. 2. Schematic diagram of the system.)

Figure 3 shows the graphical user interface (GUI) used to navigate the boat. This GUI showed the present status of the boat, such as the position, heading, speed and fan-rotation speed. It also allowed to control starting/stopping of the program. In the manual mode, the fan-rotation speeds and the winch were controlled by operating an RC transmitter.

(Fig. 3. User interface for boat navigation.)

2.2 Control Methods

Various methods for controlling unmanned moving robotic vehicles have been developed (Fossen, 1995). In some applications, the vehicle is required to move smoothly along a fixed path (Lee, Surendran, & Kim, 2009). However, the main purpose of our airboat platform was to reliably reach each target point and stop at that location. The path taken between the target points was not particularly important.

Figure 4 shows the relationship between the position of the boat and a target point. The XY coordinate system is obtained by translating the universal Mercator transverse (UTM) coordinate system to the centre of the boat. The angle between the bearing ψ_b and the heading ψ is denoted by ψ_r. The rotational speeds of the two engines were controlled in order to match the heading with the bearing. The fan-rotation speeds were determined by the maximum rotational speed $R_{\max}(D)$ of either of the two fans and the relative rotational speed $R_d(\psi_r, \dot{\psi}_r)$ of the two fans. The quantity $\dot{\psi}_r$ is the first derivative of the relative bearing ψ_r with respect to time. $R_{\max}(D)$ was determined using D, which was the distance between the boat and the target point. When the boat was far from the target point ($D > r_2$), $R_{\max}(D)$ was set at 6500 rpm in order to reach the target point rapidly. To more accurately control the boat as it approached the target point ($D < r_2$), $R_{\max}(D)$ was determined using

$$R_{\max} = \frac{6500}{d_2} D \cdot \quad (1)$$

The rotational speeds of the right and left engines (R_r, R_l) were calculated as follows:

$$R_d(\psi_r, \dot{\psi}_r) = K_p \psi_r + K_d \dot{\psi}_r . \quad (2)$$

If $R_d > 0$,

$$R_r = R_{\max}(D),\ R_l = R_{\max}(D) - R_d , \quad (3)$$

else if $R_d < 0$,

$$R_r = R_{\max}(D) + R_d ,\ R_l = R_{\max}(D) . \quad (4)$$

The proportional and derivative gain parameters K_p and K_d were determined experimentally. When $D < r_1$,

$$R_r = R_l = 0 \quad (5)$$

(i.e. the fans were stopped). When the rotational speed was set to any value less than 2000 rpm, the fans stopped because there was a centrifugal clutch on each axle. The water-quality sensor was then lowered and subsequently raised after 40 s. The index of the target point was then incremented and the boat moved in the direction of the next target point. The distances r_1 and r_2 were 5 and 6 m, respectively.

(Fig. 4. Relationship between boat and target point.)

2.3 Experimental setup

The experiment was conducted from 5 to 8 September 2010 at the Miyajimanuma mire pool, Bibai, Hokkaido, Japan. This region was originally a peat bog, but most of the surrounding land has been drained and is currently used for paddy fields. During autumn and spring, many white-fronted geese visit this region, so this pond was registered under the Ramsar Convention Treaty in 2002. Due to the inflow of fertilisers from the surrounding fields, this pond has become eutrophic and helped many aquatic plants to flourish (Toshiaki Kizuka, Yamada, & Hirano, 2008). Its area is 26 ha and its depth averages 86 cm.

The experiments were conducted as follows: First, in order to understand the dynamics of the boat, its trajectory and yaw rate were recorded for a fixed fan-rotation speed. This experiment was performed with and without the sonar transducer, because the transducer functioned as a rudder and helped the boat to cruise in a straight line. Second, a 440-m line transect was set across the middle of the pool. To investigate the spatial variability of the pool, we conducted 10-m spacing linear sampling of the pool. At each target point, the boat stopped and lowered the sensor. The trajectory of the boat was logged in order to measure the positional accuracy of each sampling point. Third, in order to acquire data for water-quality maps of the entire area, the water was again sampled over the entire area using a 40-m grid. The positional accuracy of each sampling point was also measured and logged for this exercise.

3. RESULTS AND DISCUSSION

3.1 Optimizing control of airboat

3.1.1 Relationships among rotation speed, yaw rate, drift angle and speed

The distance between the location of the GPS antenna and the centre of the boat was compensated to calculate the actual position of the centre of the boat. The speed was estimated from changes in positional data and the associated time intervals. The heading angle was obtained by the GPS compass. The yaw rate was defined by the angular speed of the heading. The drift angle β denoted the angle between the heading and the direction in which the centre of gravity moved through water.

Figure 5 shows the relationship between fan-rotation speeds and yaw rates with and without the transducer. Each bar indicates the mean yaw rate with 1-min intervals, with the error bars indicating standard deviation. The rotational speed was maintained within 100 rpm. The standard deviation of the rotational speed was 40 rpm for 6500 rpm and 100 rpm for 4000 rpm. When the difference between the rotational speeds of the two fans was increased, the yaw rates also increased. When the transducer was submerged, the yaw rates of the boat were less than those with the transducer out of water. This was due to the increased drag when the transducer was submerged, resulting in decreased yaw acceleration.

(Fig. 5. Averaged yaw rates and associated standard deviations for various combinations of fan-rotation speeds.)

It was assumed that the boat would move in a straight line when the fan-rotation speeds were equal. However, during the experiment, the boat tended to deviate randomly from a straight path. When the transducer was submerged and for all combinations of right–left fan-rotation speeds (4000–4000 rpm, 5000–5000 rpm and 6500–6500 rpm, where the first number refers to the right fan and the second to the left fan), the differences between the mean rotational speeds of each fan were less than 30 rpm. When the transducer was out of water, the boat turned in a single direction for all combinations of equal right–left fan-rotation speeds. Random disturbances such as wind and water resistance seemed to considerably affect the boat movement, and the boat also appeared to be sensitive to subtle variations in its weight distribution. These observations indicated that open-loop control of the boat was impossible and closed-loop control was necessary.

(Fig. 6. Averaged drift angles and associated standard deviations for various combinations of fan-rotation speeds.)

Figure 6 shows the drift angle β for different combinations of right–left fan-rotation speeds. The results show that the boat was continuously drifting The drift angles for right turns (0–4000, 0–5000, 0–6500) were very different from those for left turns (4000–0, 5000–0, 6500–0). For right turns, the drift angles were small, so the boat centre moved in a net forward direction. However, for left turns, the drift angles were greater than 90°, so the boat travelled backwards. This difference was caused by the asymmetric weight distribution of the boat. While the design of the boat was symmetric, the placement of sensors and batteries in the boat may have disrupted the equilibrium. In the future, such equipment shall be carefully positioned in order to enable symmetric movement.

(Fig. 7. Average speeds and associated standard deviations generated by various combinations of fan-rotation speeds.)

Figure 7 shows the relationship between the mean speeds and various combinations of right–left fan-rotation speeds, with the error bars indicating standard deviation. For all combinations of fan-rotation speeds, the speed increased with the sum of the rotational speeds of the two fans. The speed was higher when the transducer was submerged, because the absolute drift angles were smaller.

3.1.2 Accuracy of sampling position for sampling on 10-m grid

In the line transect sampling experiment, the boat automatically entered the 10-m-diameter circle, which was centred on each of the 45 points. The duration of the entire experiment was 50 min. Within this time, the boat cruised for 20 min between the sampling points and was stationary for a total of 30 min while conducting water-quality measurements.

Figure 8 shows the trajectories of the boat near three target points. The sampling position indicates the section where the sensor was lowered. When the boat entered the circles around the target points, the fans stopped. Note that even with zero fan speed, the boat continued to drift because of wind and inertia. Table 1 shows the accuracy of the sensor position with respect to the target points. The root mean square (RMS) of the distance between each target point and the sampling position was calculated and the mean RMS error was found to be 3.7 m. Therefore, we achieved the objective of maintaining the sensor position to within 5 m of the target position. The maximum and minimum RMS errors were 8.6 and 1.2 m, respectively.

(Fig. 8. Trajectories of sensor position and boat centre.)

(Table 1. RMS error between target points and sensor positions in 10-m grid sampling.)

3.1.3 Result of 40-m grid sampling

Figure 9 shows the boat trajectory and the target points for the entire area of the mire pool. The spacing between adjacent target points was 40 m. Under automatic guidance, the boat successfully reached each of the 130 target points. The boat took its first sample in the middle of the pool and then directed itself towards the east, taking samples along the way. After sampling at the boundary of the sampling zone, it turned left. (see Fig. 9, boat trajectory 1). After reaching the northern boundary and upon completion of that sample, it proceeded to the southern boundary, where the process was repeated (as shown in boat trajectories 2 and 3 of Figure 9).

The time taken for the entire area to be sampled was 231 min, excluding the time required to change the batteries and refill the fuel tank with gasoline at the shore. Within this time, the boat was in motion for 144 min and was stationary while conducting measurements for the remaining 87 min. The average travel time between the target points was 1.1 min, which was reasonable considering that the distance between the target points was 40 m. The maximum speed attained was 1.2 m s^{-1}, which is higher than the speed measured in the first experiment. The reason for this increased speed was that when the boat travelled in a straight line with feedback control, there was less resistance due to water since the submerged portion of the boat that was projected in the direction of travel had been minimised.

Table 2 shows the accuracy of the sensor position with respect to the target point. The mean RMS error was 2.6 m. The maximum and minimum RMS errors were 10.1 and 0.8 m, respectively. When the final raster map of water quality was created using sensor data, the results for the areas between the points actually sampled were derived by interpolating the sensor data of surrounding points. Therefore, if the sensor position during sampling is properly recorded, it is not critical that the water samples be taken at the exact position of the target points.

(Fig. 9. Recorded boat trajectory and target points.)

(Table 2. RMS error between target point and sensor position in 40-m grid sampling.)

3.2 Testing boat to measure water quality of the mire pool

3.2.1 Spatial variability in water quality along the transect

In the analysis of the sampled water-quality indices, the first and the last 5 s of sampling time were discarded to account for the time to lower and raise the sensor unit. The mean value of each sampling period was taken as the value for the given sampling point. At each sampling position, an average of five to six measurements was found, because the sampling time at each position was 40 s and the sampling interval was 5 s. Due to wind and inertia, there was continuous motion of the boat even during sampling. For each sample taken, the position may have therefore changed. The average position for each sampled point represents the final sample position.

In theory, reducing the spacing between the samples would produce a higher-resolution map. However, temporal changes in water quality caused by weather and water circulation limit the duration of any given experiment. Therefore, in order to minimise the effects of temporal changes in water quality, the experiment should be carried out over a period that is shorter than these natural time cycles. However, the distance between the sampling points should not be longer than the length over which spatial changes in water quality occur. A suitable balance therefore needs to be created. To this end, the scale of these spatial changes was estimated for each parameter by calculating the semivariogram of the 10-m sampling data. The semivariogram is a correlation index between two separate points (Kitanidis, 1997) and is generally used for the pre-processing of kriging interpolation. In addition, it is also useful to know the appropriate sampling spacing. Figure 10 shows several plots of empirical semivariogram data as a function of the distance between two points. The empirical semivariograms are approximated with the spherical function using Mathematica 6.0 (Wolfram Research, Inc.). The semivariogram value is small when the distance is short because closer points are more correlated. As the distance increases, the correlation decreases until the semivariogram converges to a certain value called the sill. The distance over which the variogram reaches the sill is called the range. Vertical dotted lines and associated values in Fig. 10 show the ranges for each parameter. These ranges were found to be distributed between 100 and 140 m, so the sampling spacing must be significantly less than 100 m.

(Fig. 10. Experimental semivariograms for 10-m sampling using the spherical-model approximation. Vertical dotted lines and associated values give the range over which the correlations diminish. Horizontal dotted lines indicate the sills. The parameters measured are (a) pH, (b) DO, (c) EC, (d) turbidity, (e) water temperature and (f) chlorophyll-a.)

Assuming that the sampling area is a square with area 440 × 440 m^2 (19.4 ha) and that the grid sizes are 10, 20 or 40 m, Table 2 shows the number of points, cruising distance and total time required if the sampling time per point is 40 s and the mean velocity is 0.4 m s^{-1}. With 10-m intervals, it would take about 36 h to sample a 19.4-ha area. As stated above, water quality is dynamic and may change rapidly, so sampling should be performed as quickly as possible and at least within the same day. For the pool in this study, a 40-m sampling distance was chosen. The semivariograms suggested that spatial variability of this pool could be reasonably estimated using this spacing.

(Table 3. Estimates of total time for sampling with 10-, 20- and 40-m spacing.)

3.2.2 Maps generated using 40-m sampling

Several maps generated using 40-m sampled data are shown in Fig. 11. The position data and sensor data at each target point were obtained in the same way as in the case of 10-m sampling. Interpolation was performed via the kriging method using ArcGIS 9.3.1 (ESRI, Inc.). The size of the cells in the map was 10 × 10 m^2. Coefficient of variations (CVs) were calculated in order to check the stability of the sensor values at each sampling point, and Table 4 displays the average CVs for each sensor value. The CVs of pH, DO and EC were small and stable, but those of turbidity and chlorophyll-a were large. These large CVs were attributed to the fact that turbidity and chlorophyll-a were measured optically, and might therefore fluctuate as the boat drifts during sampling.

(Table 4. Average CV for each sensor value.)

A clear frontier was observed in the water-temperature map [Fig. 11(a)] because, as shown in Fig. 9, the starting point was in the middle of the pool. The boat started at 07:22 (morning) and finally stopped at 13:12 (afternoon). During these 6 h, the water was warmed by sunlight, so a 4.1 °C difference in water temperature was observed between the start and end points. A frontier was also observed in the EC map [Fig. 11 (b)]. However, EC is not usually affected by temperature, so another reason such as water circulation is likely. The EC was higher at the western side of the pool and lower at the eastern side. Because this pool had inlets on the western border, as shown in Fig. 11(b), the EC distribution was attributed to the dissolved fertilisers entering the pool from these inlets. Therefore, it was concluded that the map adequately described the EC distribution of the pool. The turbidity map did not have a clear frontier [Fig. 11(c)]. It was, therefore, concluded that turbidity was not influenced by sunlight or temperature change. The turbidity levels were higher on the east side of the pool than on the west side. On the day of the experiment, the winds blew from west to east, so the spatial unevenness in the turbidity was attributed to the water flow caused by wind.

During daylight hours, changes in sunlight and temperature are unavoidable, and because photosynthesis affects pH and DO levels, these parameters will also change. Therefore, to reduce changes in temperature and eliminate problems caused by sunlight, an ideal time for measurements would be at night. It is not practical for a person to row a boat while taking samples for several hours during the night, but this can easily be done using an unmanned robotic boat navigated by GPS. Moreover, the wind is generally less at night, so it is expected that the water-quality data would be temporarily stabilised as a result of minimal disturbances of water.

(Fig. 11. Maps resulting from 40-m grid sampling: (a) water temperature, (b) EC and (c) turbidity.)

4. CONCLUSIONS AND FUTURE WORK

We developed an unmanned robotic airboat to perform grid sampling of the water quality of a mire pool. This boat can approach target points automatically even while the wind is blowing. On the basis of our results, the precision of the sampling positions is deemed acceptable.

However, certain problems were encountered: the boat occasionally swayed from side to side. In order to eliminate this oscillation, the engine-control frequency should be increased and the gain values that determine the fan-rotation speeds in Eq. (2) should be carefully adjusted. It would be useful to perform a dynamic simulation of the boat in order to determine the optimal control parameters. When taking side-scan sonar measurements to create a profile of the bottom of a lake, it is ideal to drive the boat in a stable straight line, which may require a rudder. However, such a rudder would require a mechanism to prevent it from becoming tangled in aquatic weeds.

Using grid sampling, fine-resolution water-quality distribution maps were obtained. This technique will help hydrologists to understand the water circulation system of this pool and to predict its future status. However, temperature and other water-quality parameters changed during the sampling process. Therefore, sampling should be performed at night in order to take full advantage of the automatic unmanned airboat. Finally, although parallel paths were used in this experiment, spiral or other types of paths may be more appropriate to mitigate the temporal variations in the water-quality parameters.

ACKNOWLEDGEMENTS

The authors gratefully acknowledge Dr Kizuka, Mr Mochizuki, Mr Nakanishi and Mr Fujishima of Hokkaido University and Dr Ushiyama of the Miyajimanuma Waterbird & Wetland Center for their assistance in carrying out the experiments. We also thank Mr Nishiyama of Mtech Co. for his assistance in developing the ECU. This study was supported by Grant-in-Aid for Scientific Research (A) 20248207.

REFERENCES

Banzi, M. (2009). *Getting Started with Arduino*. Tokyo: O'Reilly Japan.

David, C., Twichell, B. D., Andrews, H., Edmiston, L., & Stevenson, W. R. (2007). Geophysical Mapping of Oyster Habitats in a Shallow Estuary; Apalachicola Bay, Florida. *U.S. Geological Survey Open-File Report, 2006-1381*.

Fossen, I. T. (1995). *Guidance and Control of Ocean Vehicles*. West Sussex: John Wiley & Sons Ltd.

Kitanidis, P. K. (1997). *Introduction to geostatistics: applications to hydrogeology*. Cambridge: Cambridge University Press.

Kizuka, T., Yamada, H., & Hirano, T. (2008). Hydrochemistry of Miyajimanuma Pool in the Ishikari Peatland, Northern Japan. *Papers on Environmental Information Science, 22*, 493-498.

Kizuka, T., Yamada, H., Yazawa, M., & Chung, H. H. (2008). Effects of agricultural land use on water chemistry of mire pools in the Ishikari Peatland, northern Japan. *Landscape and Ecological Engineering, 4*(1), 27-37.

Lee, G., Surendran, S., & Kim, S. H. (2009). Algorithms to control the moving ship during harbour entry. *Applied Mathematical Modelling, 33*(5), 2474-2490.

Li, C. Y., & Weeks, E. (2009). Measurements of a small scale eddy at a tidal inlet using an unmanned automated boat. *Journal of Marine Systems, 75*(1-2), 150-162.

Singh, A., Stealey, M. J., Chen, V., Kaiser, W. J., Batalin, M., Lam, Y., et al. (2007). Human assisted robotic team campaigns for aquatic monitoring. *Journal of Field Robotics, 24*(11-12), 969-989.

Singh, K., Worley, J., & Risse, M. (2008). Sludge Measurement Using Global Positioning System (GPS) Enabled Sonar Equipped Airboat in a Lagoon. *Applied Engineering in Agriculture, 24*(5), 603-609.

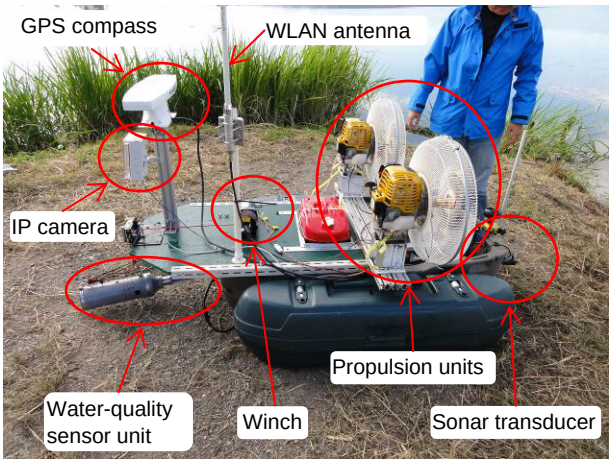

Fig. 1. Unmanned boat platform.

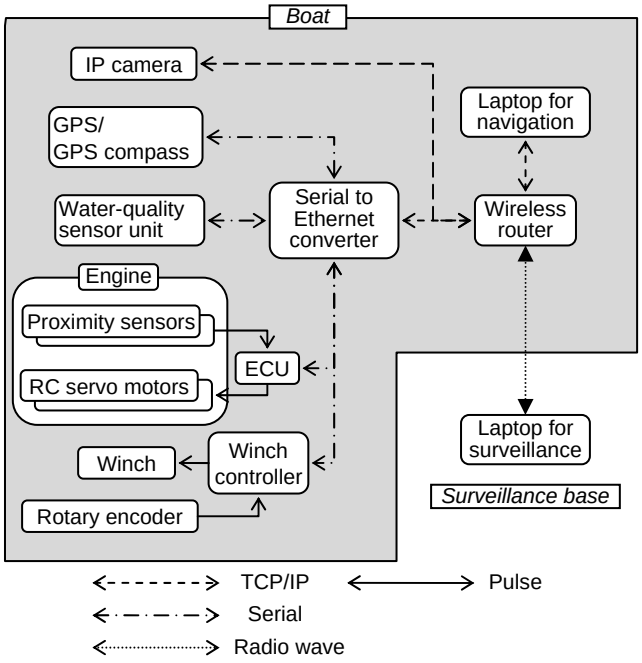

Fig. 2. Schematic diagram of the system.

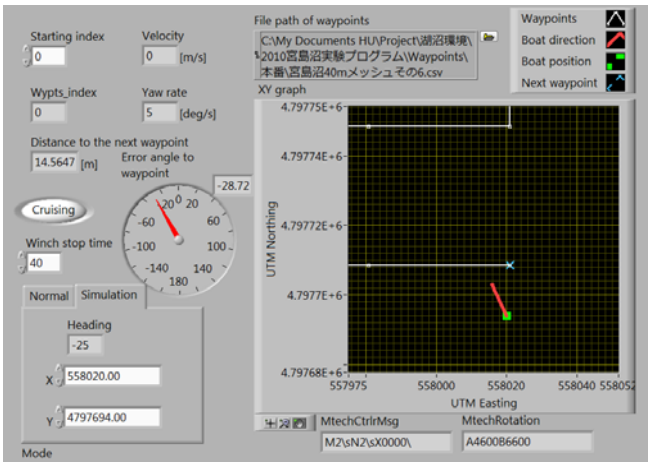

Fig. 3. User interface for boat navigation.

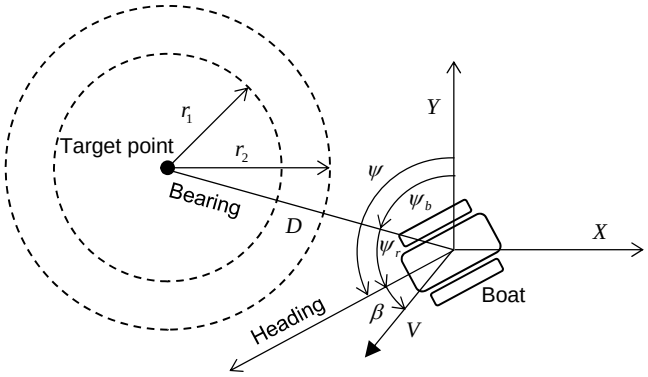

Fig. 4. Relationship between boat and target point.

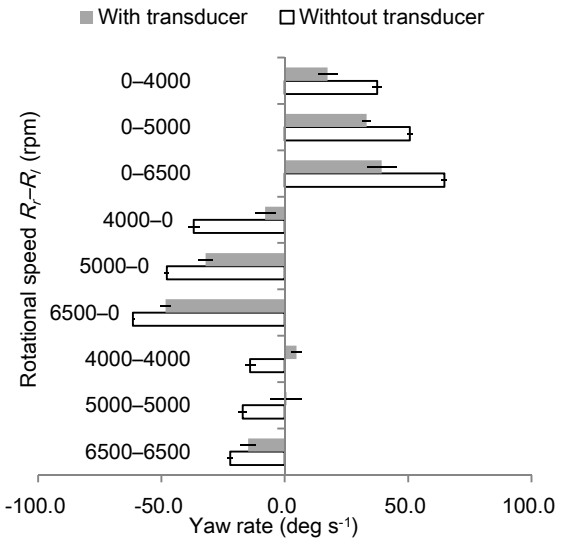

Fig. 5. Averaged yaw rates and associated standard deviations for various combinations of fan-rotation speeds.

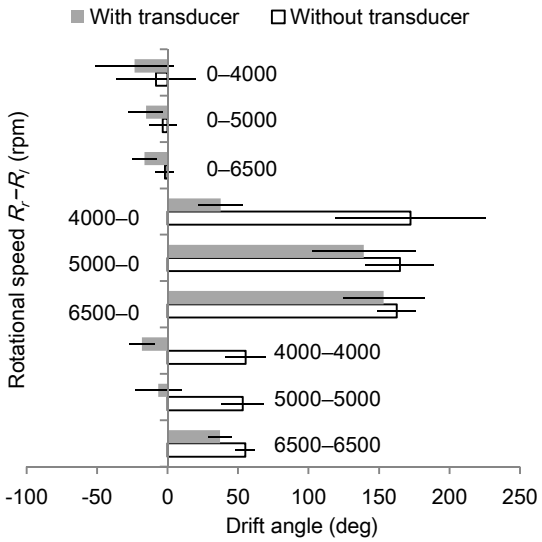

Fig. 6. Averaged drift angles and associated standard deviations for various combinations of fan-rotation speeds.

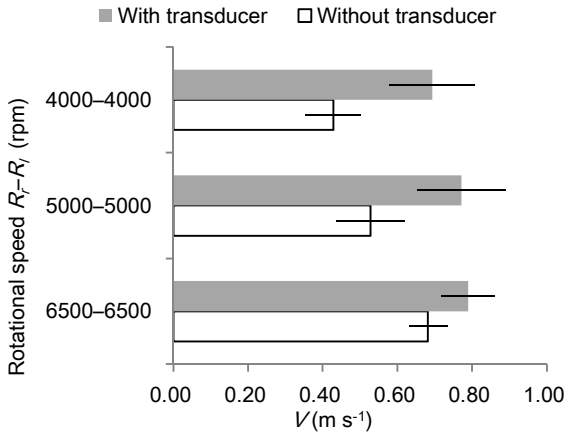

Fig. 7. Average speeds and associated standard deviations generated by various combinations of fan-rotation speeds.

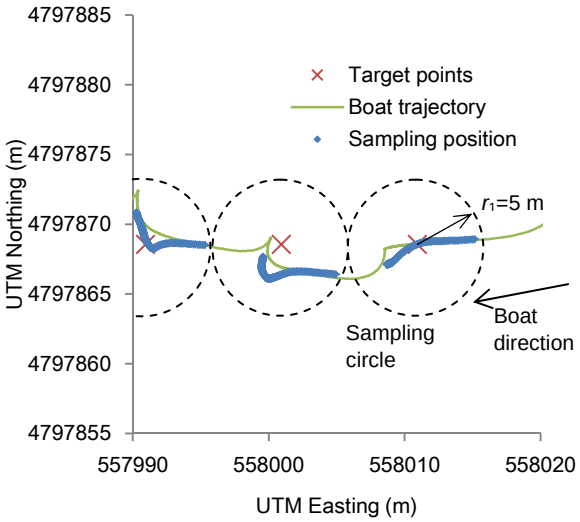

Fig. 8. Trajectories of sensor position and boat centre.

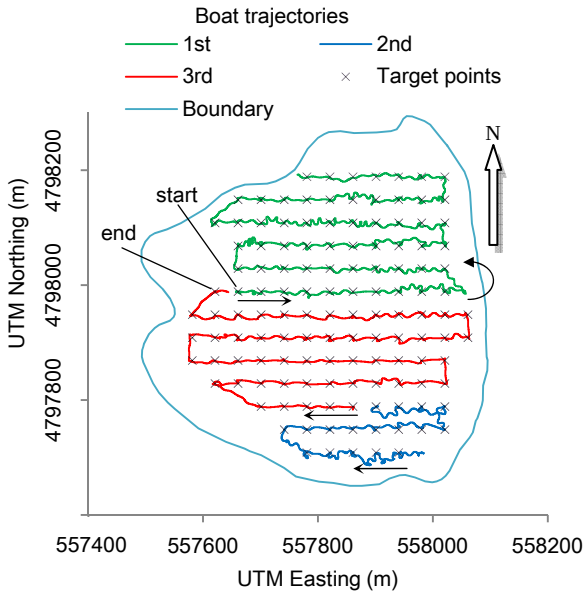

Fig. 9. Recorded boat trajectory and target points.

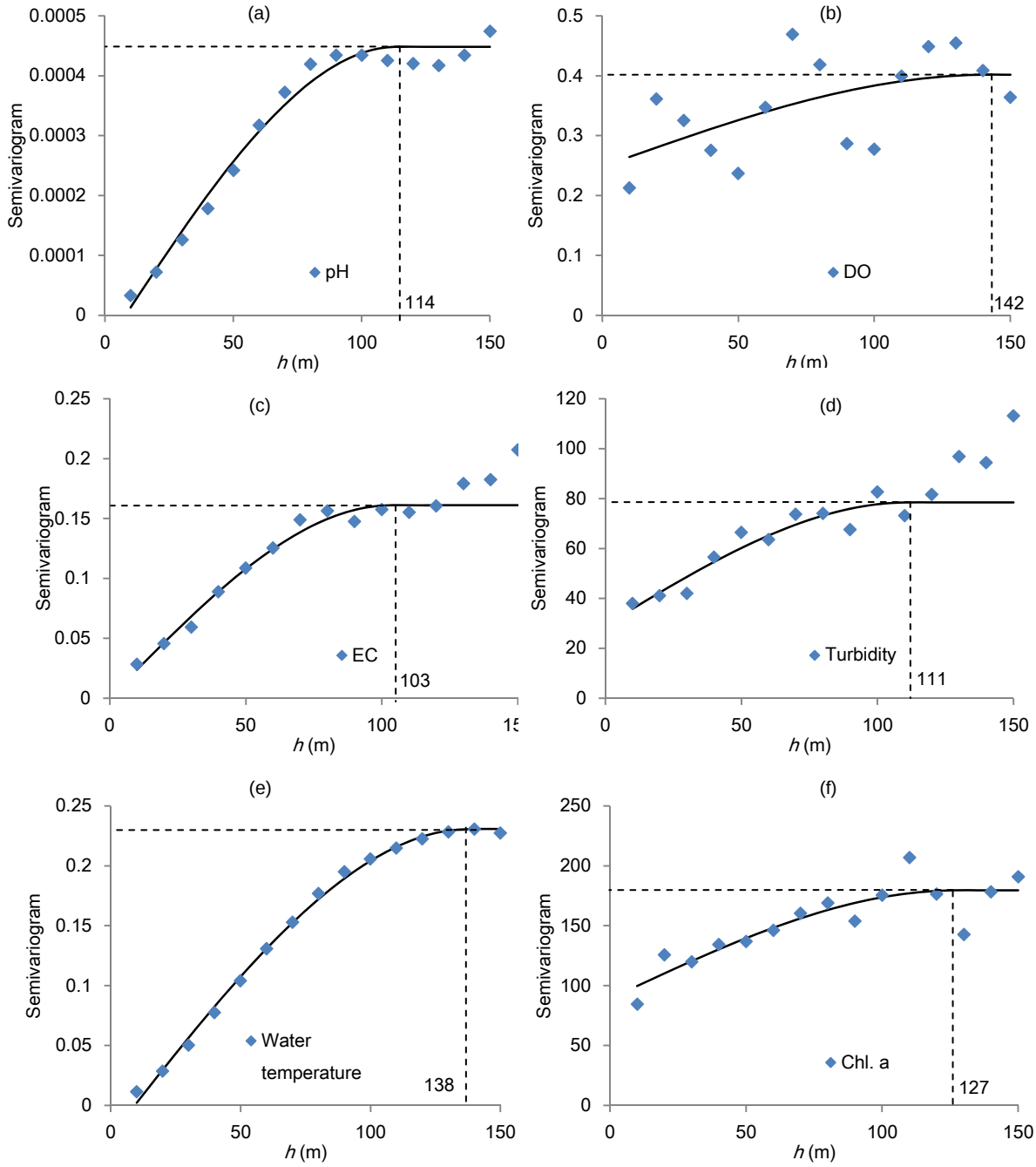

Fig. 10. Experimental semivariograms for 10-m sampling using the spherical-model approximation. Vertical dotted lines and associated values give the range over which the correlations diminish. Horizontal dotted lines indicate the sills. The parameters measured are (a) pH, (b) DO, (c) EC, (d) turbidity, (e) water temperature and (f) chlorophyll-a.

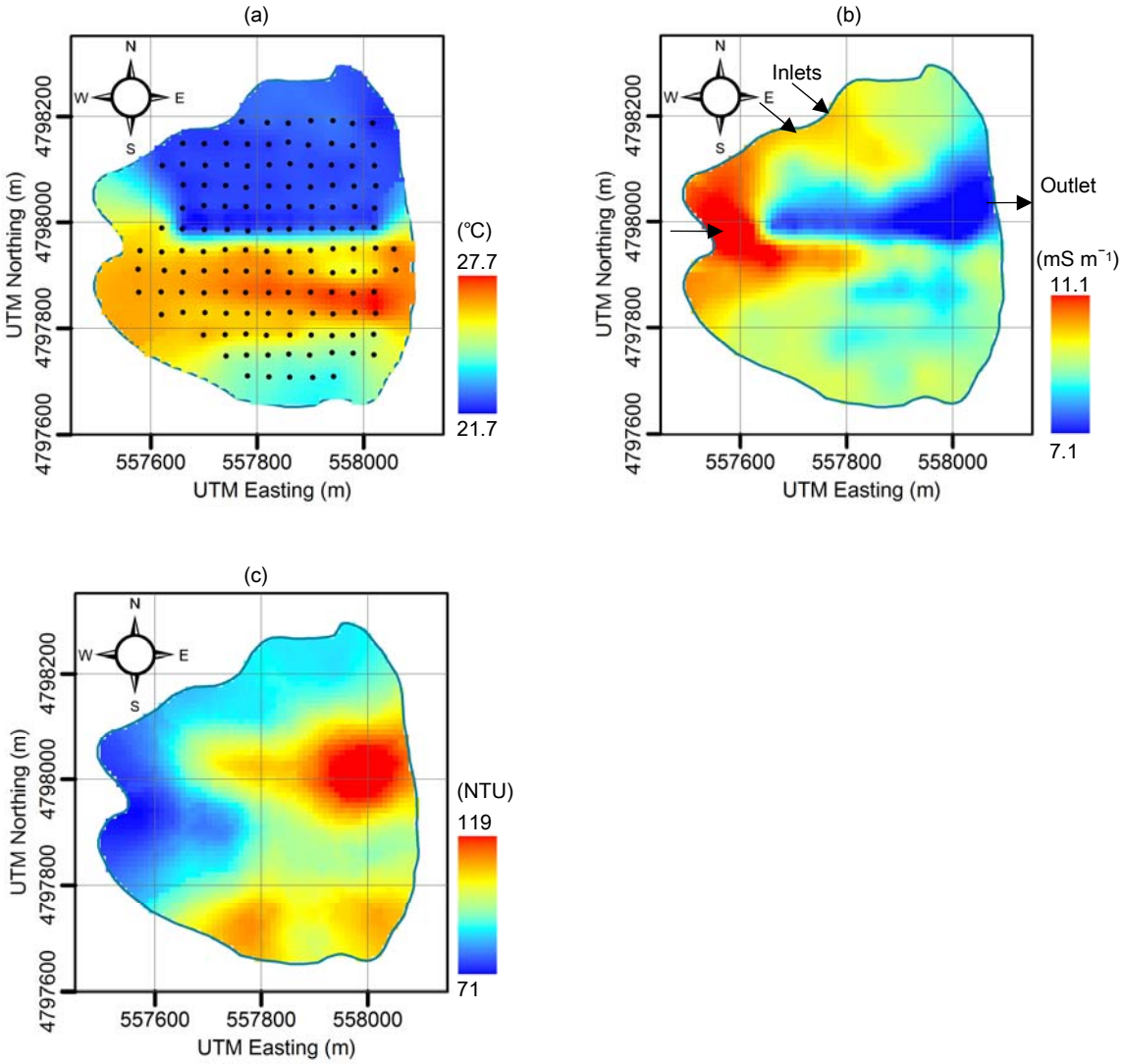

Fig. 11. Maps resulting from 40-m grid sampling: (a) water temperature, (b) EC and (c) turbidity. Black dots in (a) indicate sample positions.

Table 1. RMS error between target points and sensor positions in 10-m grid sampling.

Mean RMS	3.7 m
Maximum RMS	8.6 m
Minimum RMS	1.2 m

Table 2. RMS error between target point and sensor position in 40-m grid sampling.

Mean of RMS	2.6 m
Maximum RMS	10.1 m
Minimum RMS	0.8 m

Table 2. RMS error between target point and sensor position.

Mean of RMS	2.6 m
Maximum RMS	10.1 m
Minimum RMS	0.8 m

Table 4. Average CV for each sensor value.

	Average CV (%)
pH	0.2
DO	2.1
EC	1.4
Turbidity	25.9
Water temperature	0.3
Chlorophyll-a	78.7